2007

The Effect of the Size of Pinning Centres on the Critical Current Density in High-Temperature Superconductors

Salama Bakhit Sowaidan Al-neaimi

United Arab Emirates University

Deanship of Graduate Studies

The Effect Of The Size Of Pinning Centres On The Critical Current Density In High-Temperature Superconductors

By

Salama Bakhit Sowaidan Al neaimi

Supervised by

Dr. Maamar Benkraouda

Physics Department

College of Science, UAEU

Dr. Ihab Obaidat

Physics Department

College of Science, UAEU

Dr. Usama Al Khawaja

Physics Department

College of Science, UAEU

A thesis submitted to the Deanship of Graduate Studies in Partial fulfilment of the Requirements for Degree of Master of Science in

Materials Science and Engineering

2006-2007

ES/F11

United Arab Emirates University
Graduate Studies
M.S.c. Program in Materials Science and Engineering

THESIS EXAMINATION REPORT

Student ID : 200270213
Student Name : Salama Bakhit Sowaidan Alneaimi

Title of The Thesis : The effect of the size of pinning centers on the critical current density in high temperature superconductor.

The Thesis Examination as A Partial Fulfillment of M. Sc. Degree in Materilas Science and Engineering Was conducted on ..... Based on Examining the Thesis and the Students Presentation and the Subsequent Discussion, The Committee Recommends:

- [x] Thesis is Satisfactory as is.
- [ ] Thesis is Satisfactory After Minor Modifications.
- [ ] Thesis should be Re-Evaluated After Major Modifications.
- [ ] Thesis is Rejected

Examining Committee Members:

Thesis Supervisor: Name: Haamor Bentzeouh Signature: ..... Date: 14-12-06

Member : Name: Ihab Obaidat Signature: Ihab Obaidat Date: 14-12-06

Member : Name: Usama Al Khawaja Signature: ..... Date: 14-12-06

Member : Name: Fathalla Hamed Signature: ..... Date: 14-12-06

Member : Name: Mousa Hussein Signature: ..... Date: 14-12-06

Approval of Program Coordinator:

Dr. Mousa Hussein ..... Date: 18-12-2006

APPROVAL:
Dean of Graduate Studies James E. Metcker Date: .....

عميد الدراسات العليا — جامعة الإمارات العربية المتحدة — Dean of Graduate Studies — U.A.E. UNIVERSITY

Dedication

This thesis and all my success is dedicated to my beloved parents, my husband and sons

Abdullah

&

Hamad

Abstract

Superconductor materials that have no resistance to the flow of electricity are one of the last great frontiers of scientific discovery.

Superconductivity in these materials occurs particularly in the copper-oxide (CuO_2) planes. However, since these materials are type-II superconductors, magnetic fields can penetrate these materials in quantized amounts of flux called vortices without completely destroying superconductivity, but producing some resistance, due to vortex motion. In order to overcome the resistance problem, vortices must be pinned to prevent their motion and hence eliminate the resistance.

In this work study we have performed extensive numerical simulations to study the effect of the size of pinning centres on the critical current density of driven vortex lattices interacting with square periodic arrays of pinning sites. This has been carried out at different temperatures and for several values of pinning strengths. We have solved the over damped equation of vortex motion taking into account the vortex-vortex repulsion interaction, the attractive vortex-pinning interaction, the thermal force, and the driving Lorentz force.

We have found that, while the critical current density increases with pinning size at high temperatures, it is almost independent of pinning size at low temperatures. We have also found that increasing the size of the pinning centres suppresses the rate at which the critical current density decreases with temperature.

Acknowledgments

I owe great thanks to the United Arab Emirates University that offered me this opportunity to enrol in the Master Program. I also would like to thank my supervisors Dr. Maamar Benkraouda, Dr. Ihab Obaidat and Dr. Osama Al Khawaja for their patient and understanding and for the great help they provided me in my thesis.

Special appreciation is expressed to my colleagues and friends in the UAE University, especially my dear friends Bakhita and Hessa for their great help and support.

Special acknowledgement to my parents, sisters and brothers who provided me with their continuous encouragement and support, especially my sister Shamma, for her great help especially in designing the presentation, my mother and sister Yammna for taking care of my sons during my work on this thesis.

Table of Contents

Abstract iii
Acknowledgments iv

Chapter **Page**
List of figures .....

Chapter 1: Introduction to superconductivity
1. Introduction 2
2. The basic quantities T_c, H_c and J_c 2
3. Two kind of superconductors 4
4. Flux quantization and Josephson Effect 4
5. Theories of superconductivity 5
   5.1. London theory 5
   5.2. The BCS theory 6
   5.3. Ginzburg-Landau theory 7
6. Type II superconductivity 9
   6.1. The electromagnetic region (λ) and core region (ξ) of a single Abrikosov vortex 10
   6.2. The lower critical magnetic field 12
   6.3. The upper critical magnetic field 13
   6.4. Vortex pinning 13
   6.5. The resistive state of type II superconductor 15
7. High temperature superconductivity 16
   7.1. Features of High-temperature superconductors 17

Chapter 2: Numerical Method
1. Introduction 20
2. The system 22
3. The equation of motion 23
   3.1. The vortex-vortex force 23
   3.2. The vortex-pin force 24
   3.3. The driving force 24
   3.4. Effect of the temperature 25
4. The numerical method 25

Chapter 3: Results and discussion
1. Introduction 29
2. The vortex average velocity $\bar{v}_x$ versus the driving force f_d 30
3. The dependence of the critical depinning force F_d^c on temperature 38
4. The effect of the pinning size on the critical depinning force F_d^c 41

Conclusions 45
References 46

List of Figures

Figure title **Page**

Figure 1.1: The temperature dependence of the critical field H_c. 3

Figure 1.2: The phase diagram of a typical type II superconductor. 10

Figure 1.3: A schematic diagram of the distributions of the order parameter $\Psi(\rho)$, the magnetic field $H(\rho)$ and the current density $J(\rho)$ near a single Abrikosov vortex. 11

Figure 2.1: (a) Schematic plot of square pinning sites represented by circles and vortices represented by dots.(b) Vortex-vortex and vortex pin forces. 22

Figure 2.2: The average velocity $\bar{v}_x$ vs. the driving force f_d at different temperatures. 27

Figure 3.1: The average velocity $\bar{v}_x$ vs. the driving force f_p at two different temperatures. 31

Figure 3.2: The average velocity $\bar{v}_x$ vs. the driving force f_d for $f_p=1$, for different r_p and different temperatures. 33

Figure 3.3: The average velocity $\bar{v}_x$ vs. the driving force f_d for $f_p=3$, for different r_p and different temperatures. 34

Figure 3.4: The average velocity $\bar{v}_x$ vs. the driving force f_d for $f_p=5$, for different r_p and different temperatures. 35

Figure 3.5: Calculation of F_d^c from the $\bar{v}_x$ vs. f_p curve 37

Figure 3.6: The critical depinning force F_d^c as a function of temperature for several values of the radius of the pinning center r_p and pinning strength f_p. 40

Figure 3.7: The critical depinning force F_d^c as a function of the radius of the pinning center r_p. the pinning strength f_p is fixed for all curves in the sub figures. 43

Figure 3.8: The critical depinning force F_d^c as a function of the radius of the pinning center r_p. the temperature is fixed for all curves in the sub figures. 44

Chapter 1

Introduction to superconductivity

1- Introduction

Superconducting is a new state of matter, it was known by Kammerlingh Onnes in 1911 [1]. In 1908 Kammerlingh Onnes liquefied helium, after three years; in 1911 he found that the resistance of mercury, Hg, dropped to zero at temperature below 4.19 K. The most important thing was that the resistance drop was discontinuous, which means that a phase transition to new state with zero resistance took place. The temperature of this phase transition was called the critical temperature T_c. Lead (Pb) and Tin (Sn) also give the same transitions. The highest T_c was 23.2 K for Nb_3Ge until the discovery of a new class of so-called high-temperature superconductors in 1986.

The superconductivity was found to be destroyed by heating the sample above its critical temperature and by applying a magnetic field above a value called the critical magnetic field. The behaviour of a superconductor in a magnetic field has become the subject of systematic study, especially after the discovery of type II superconductors in 1960.

2- The basic quantities T_c, H_c and J_c

The thermodynamic critical field H_c is an important magnetic characteristic of a superconductor. In 1933 Meissner and Ochsenfeld found that when a superconductor is cooled below T_c in a weak magnetic filed $H < H_c$, the field is expelled from the sample. This perfect diamagnetism is called the Meissner effect [2]. The physical explanation is that screening supercurrents flow in a thin surface layer of sample, producing a magnetic field which exactly cancels the external field. As a result, the magnetic field inside a superconductor is zero. At $H > H_c$ the superconducting state is unstable and a transition to

normal state with finite resistance occurs. Figure 1.1 shows the relation between H_c and temperature.

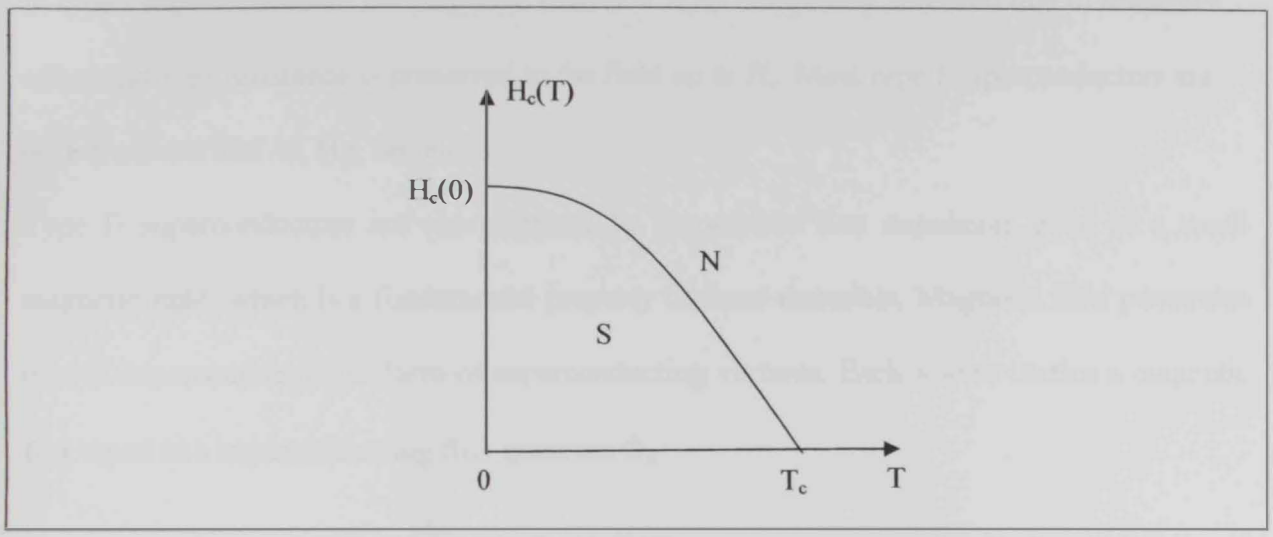

Figure 1.1: The temperature dependence of the critical field H_c.

(S is the superconducting state, and N is the normal state)

Another important characteristic of a superconductor is the maximum possible transport current density J_c, which can flow without dissipation. According to Silsbee's criterion, a superconductor loses its zero resistance when at any point on the surface the total magnetic field strength, due to the transport current and applied magnetic field, exceeds the critical field strength H_c. This quantity J_c is called the thermodynamic critical current density or the depairing current and depends on the external magnetic field and temperature.

Because of the penetration of magnetic flux into the superconductor at magnetic field lower than H_c, J_c for most practical superconductor is much smaller than the thermodynamic critical current density. In this respect, according to Abrikosov (1952), superconductors are classified into two kinds: type I and type II superconductors

3- Two types of superconductors

In type I superconductors the magnetic field $H < H_c$ is completely screened due to Meissner effect and zero resistance is preserved in the field up to H_c. Most type I superconductors are pure elements like Al, Hg, Sn, etc.

Type II superconductors are characterized by incomplete flux expulsion, even in a small magnetic field, which is a fundamental property of these materials. Magnetic field penetrates type II superconductors in form of superconducting vortices. Each vortex carries a magnetic flux equal to a superconducting flux quantum Φ_o

$$\Phi_o = \frac{hc}{2e} \approx 2.07 \times 10^{-15} Wb \qquad (1.1)$$

where h is plank's constant 6.6262 x 10^{-34} J s and e is the charge of an electron 1.60219 x 10^{-19} C.

These vortices move under external current generating an electric field. Therefore, zero resistance state does not occur in the sample because of the motion of the magnetic vortices. For practical applications it is important to have zero resistance superconductor materials. This is attained if the vortices are prevented from moving. This effect is called vortex pinning.

4- Flux quantization and Josephson effect

The first quantum nature of Superconductivity is the flux quantization. If a superconducting ring carries a supercurrent, magnetic flux inside the ring can have only values which are integer multiples of a superconducting flux quantum Φ_o. Thus Φ_o is the unit of magnetic flux distributing within a superconductor [3].

Another quantum nature of superconductivity is the Josephson Effect. If two superconductors are brought into weak electrical contact then nondissipative superconducting current can flow through such contact with zero voltage drops [4].

5- Theories of superconductivity

Since the discovery of superconductivity, great efforts have been devoted to explain the remarkable properties of superconductors. The most important theories are London, the BCS and Ginzburg-Landau theories.

5.1 London theory

In 1935, after the discovery of Meissner effect, London brothers developed a phenomenological theory of superconductivity, which is referred to as London theory [5, 6, 7, 8, 9, and 10]. London theory which deals with the electrodynamics behaviour of superconductors on macroscopic scale was capable of describing a large number of observations. The two basic equation of the London theory are:

$$\frac{d}{dt}(\Lambda\vec{j}) = \vec{E}, \qquad (1.2)$$

$$curl(\Lambda\vec{j}) = -h, \qquad (1.3)$$

where $\Lambda = \frac{m}{n_s e^2}$ is the screening length and m, n_s, and e are the mass, the number per unit volume, and charge of carriers of the super current, respectively. Equation (1.2) means that the change of the current density with time is proportional to the electric field $\vec{E}$ [7], and equation (1.3) describes the Meissner effect in quantitative way [5, 7]. The most important

conclusions of London theory are: I. The decay of the external field of order λ_L in the surface layer of the superconductor. II. The magnetic flux quantization, which was experimentally confirmed in 1961. In spite of the importance of the observation of London theory, it could not give any explanations about the origin of superconductivity on the microscopic scale.

5.2 The BCS theory

The understanding of the theory of superconductivity was advanced in 1957 by three American physicists; John Bardeen, Leon Cooper, and John Schrieffer through their famous theory of superconductivity which is known as the BCS theory [8, 11, 12]. A key conceptual element in the BCS theory is the pairing of electrons (Cooper pair) [5]. This Cooper-pairing results from the slight attraction between the electrons mediated by lattice vibrations (phonon interaction).

Pairing of electrons can behave very differently from single electrons, they do not obey the Pauli Exclusion Principle, but they can condense into the same energy level. The electron pairs have a slightly lower energy and leave an energy gap above them of order of 0.001 eV which inhibits the kind of collision interactions which lead to ordinary resistivity. For temperatures such that the thermal energy is less than the band gap, the material exhibits zero resistivity.

Bardeen, Cooper, and Schrieffer received the Nobel Prize in 1972 for the development of theory of superconductivity.

5.3 Ginzburg-Landau theory

Ginzburg-Landau theory is a mathematical theory used to model superconductivity. This theory was published by Ginzburg and Landau in 1950 and was extended in a subsequent microscopic theory by Gor'kov during 1950-1960, based on BCS theory.

Ginzburg and Landau argued that the free energy F of a superconductor near the superconducting transition can be expressed in terms of a complex order parameter ψ [5, 8], which describes how deep into the superconducting phase the system is. The free energy has the form:

$$F = F_n + \alpha|\psi|^2 + \frac{\beta}{2}|\psi|^4 + \frac{1}{2m}|(-i\hbar\nabla - 2e\mathrm{A})\psi|^2 + \frac{|\mathrm{H}|^2}{2\mu_o}\psi \qquad (1.4)$$

where F_n is the free energy density of the normal phase, α and β are phenomenological parameters depending on the temperature and the material, **A** is the electromagnetic vector potential, m and e are the mass and charge of the electron respectively and H is the external magnetic field. Integrating equation (1.4) over the sample volume gives the free energy. By minimizing the free energy with respect to fluctuations in the order parameter and the vector potential, we get the two Ginzburg-Landau equations:

$$\alpha\psi + \beta|\psi|^2\psi + \frac{1}{2m}(-i\hbar\nabla - 2e\mathrm{A})^2\psi = 0 \qquad (1.5)$$

$$\mathrm{J} = \frac{2e}{m}(\psi^*(-i\hbar\nabla - 2e\mathrm{A})\psi) \qquad (1.6)$$

where **J** is the electrical current density. The first equation determines

based on the applied magnetic field. The second equation provides the superconducting current [8].

The Ginzburg-Landau equations provide many important results. The most important result is its prediction of the existence of two characteristic lengths in a superconductor.

The first is the coherence length ξ, given by

$$\xi = \sqrt{\frac{\hbar^2}{2m|\alpha|}} \qquad (1.7)$$

which describes the size of thermodynamic fluctuations in the superconducting phase. ξ characterizes the distance over which ψ decreases to zero . The second is the penetration depth λ, given by

$$\lambda = \sqrt{\frac{m}{4\mu_o e^2 \psi_o^2}} \qquad (1.8)$$

where ψ_o is the equilibrium value of the order parameter in the absence of an electromagnetic field. The penetration depth describes the depth to which an external magnetic field can penetrate the superconductor [10, 13, 14].

The ratio $\kappa = \lambda/\xi$ is known as the Ginzburg-Landau parameter. For type I superconductors $\kappa < 1/\sqrt{2}$, and for type II superconductors $\kappa > 1/\sqrt{2}$. For type II superconductors, the phase transition from the normal state is of second order, for type I superconductors it is of first order in an applied magnetic field. The most important finding from Ginzburg-Landau theory was made by Alexei Abrikosov in 1957. In a type II superconductor in a relatively high magnetic field- the field penetrates in quantized tubes of flux, which form a hexagonal arrangement in clean sample.

6- Type II superconductivity

The value of the Ginzburg-Landau (GL) parameter $\kappa > 1/\sqrt{2}$, characterizes type II superconductors. Another characteristic is that if a specimen is placed in magnetic field, it does not exhibit total flux expulsion except for very low fields [15]. The penetration field is called the lower critical magnetic field H_{c1} and it is smaller than the thermodynamic critical field H_c. H_{c1} can be small as 10-100 G, whereas H_c is of order of 10^3 G.

Figure 1.2 shows a typical H-T phase diagram for type II superconductor of an ideal cylindrical shape. For $H < H_{c1}$ there is complete flux expulsion (Meissner phase). For $H_{c1} < H < H_{c2}$ magnetic flux penetrates a superconductor but the penetration is incomplete. Complete penetration of a flux takes place at a much higher field H_{c2} which is called the upper critical magnetic field. In the field range $H_{c1} < H < H_{c2}$ the superconductor is described to be in the mixed state. According to Abrikosov's theory, the mixed state results from the penetration of magnetic vortices into a superconductor. Each magnetic vortex carries the flux quantum Φ_0. A superconductor in this region contains finite amount of vortex lines. In equilibrium conditions and in clean samples the vortices form regular vortex lattice. The existence of the vortex lattice was first confirmed by Träuble and Essman in 1967 [16].

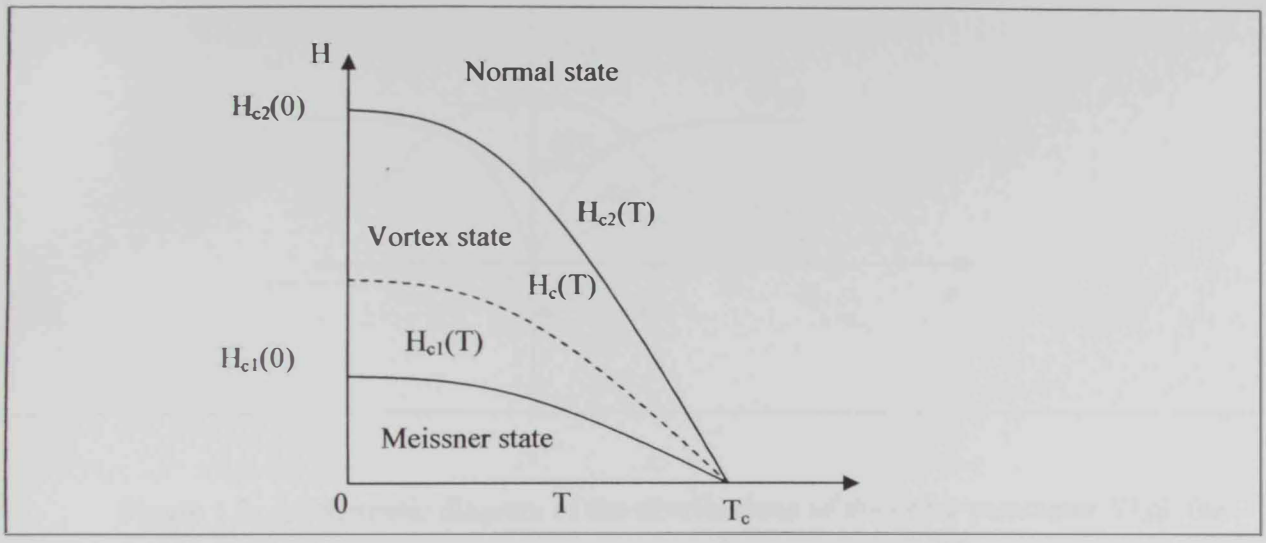

Figure 1.2: The phase diagram of a typical type II superconductor.

6.1 The electromagnetic region (λ) and core region (ξ) of a single Abrikosov vortex

The structure of a single Abrikosov vortex in a homogeneous bulk type II superconductors is shown in Figure 1.3. The magnetic field is maximum near the center of the line and exponentially decays with distance from the center over the characteristic length λ (the penetration depth). The order parameter $\psi(\rho)$ is reduced in a small core region of radius of the order of the coherence length ξ; therefore the vortex core can be qualitatively represented as a region of normal phase of cross sectional area ~ ξ^2. Physically, the reduction of the order parameter in the vortex core is due to large depairing currents flowing near the centre of the vortex line.

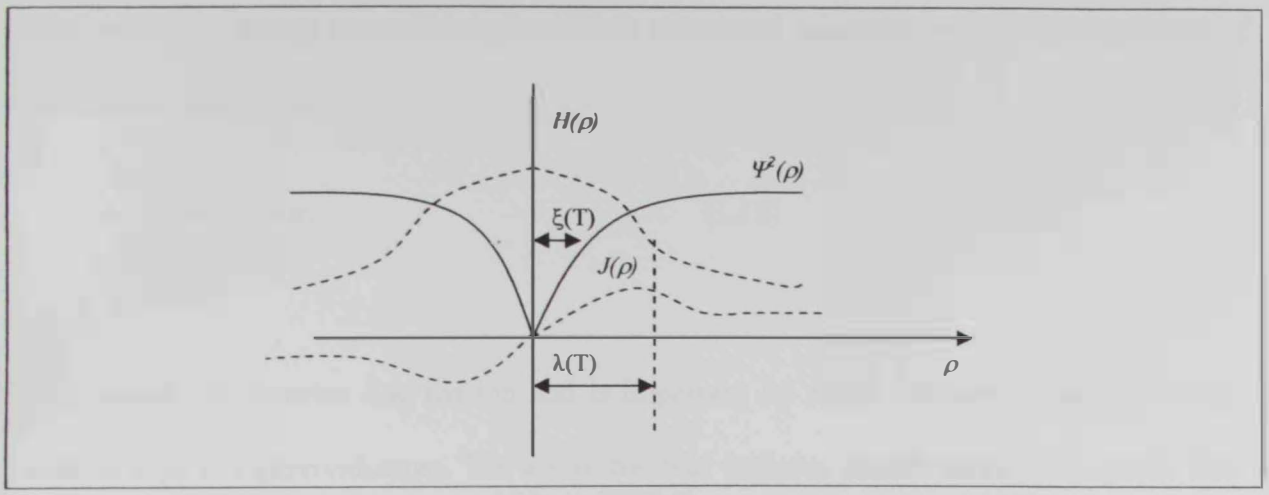

Figure 1.3: A schematic diagram of the distributions of the order parameter $\Psi(\rho)$, the magnetic field $H(\rho)$ and the current density $J(\rho)$ near a single Abrikosov vortex.

Mathematically the magnetic field distribution near the vortex line H can be written in the form

$$H + \lambda^2 curlculrH = \Phi_0 \delta(\rho) e_\upsilon \qquad (1.9)$$

where e_v is a unit vector directed along the vortex line, $\delta(x)$ is the delta-function and ρ is the distance from the core, and the normalization factor Φ_0 reflects the fact that the vortex carries exactly one magnetic flux quantum. The solution of equation (1.9) is:

$$H_\upsilon = \frac{\Phi_o}{2\pi\lambda^2} \mathrm{K}_o\left(\frac{\rho}{\lambda}\right) \qquad (1.10)$$

where K_0 is the zero-order Bessel function of an imaginary argument.

The vortex line energy per unit length ε can be calculated using the free energy functional of the London theory and is given by:

$$\varepsilon = \left(\frac{\Phi_o}{4\pi\lambda}\right)^2 \ln\kappa. \qquad (1.11)$$

This quantity is a vortex line tension and is important for many estimates regarding energy scale in type II superconductors. The above formula includes contributions of magnetic field and electric currents to the total energy of vortex. An additional contribution is the core energy which is given by the superconducting condensation energy within the vortex. Exact numerical integration of GL equations leads to the following expression for the total energy

$$\varepsilon = \left(\frac{\Phi_o}{4\pi\lambda}\right)^2 (\ln\kappa + \alpha) \qquad (1.12)$$

where $\alpha \sim 0.5$ represents the core contribution to the vortex energy [17].

6.2 The lower critical magnetic field

The lower critical magnetic field H_{c1} is the magnetic field strength where the Meissner effect is destroyed and vortices of cylindrical shape start to penetrate into the bulk of a type II superconductor. It is given by

$$H_{c1} = \frac{4\pi\varepsilon}{\Phi_o} \approx \frac{\Phi_o}{4\pi\lambda^2}\ln\kappa \qquad (1.13)$$

where the core contribution is neglected. For $T = 0$ the relation between H_{c1} and H_c has the form $H_{c1}/H_c = \ln\kappa/\sqrt{2}\kappa$.

6.3 The upper critical magnetic field

The high magnetic field strength up to which the mixed state can persist is called the upper critical magnetic field H_{c2}. H_{c2} can be estimated from using GL theory [18] as:

$$H_{c2}(T) = \sqrt{2}\kappa H_c(T) = \frac{\Phi_o}{2\pi\xi^2(T)} \qquad (1.14)$$

This suggests that materials with a high value of k remain in the mixed state until quite strong magnetic fields are applied. Physically H_{c2} corresponds to the onset of the overlap between the vortex cores. The upper critical field was found to grow with T_c of a superconductor and can be of the order of 20 - 40 T for commercially available superconductors.

For $H > H_{c2}$ a macroscopic sample does not show flux expulsion; however a superconducting phase still remains in thin surface layer of the order of $\xi(T)$. This surface superconductivity exists in an interval $H_{c2} < H < H_{c3}$, where the so-called surface nucleation field $H_{c3} \approx 1.69H_{c2}$ [19].

6.4 Vortex pinning

There are two types of pinning forces; the elementary pinning force and the bulk pinning force density. An example of elementary pinning force is the interaction between a flux line and a void which may be present due to the manufacturing process of type II material. When a vortex passes through the void, its energy is lowered by roughly the product of the condensation energy density and the void dimensions. In practical superconductors, defects

which act as pinning centers include various lattice defects, nonsuperconducting precipitates, grain boundaries, dislocations, etc.

The bulk pinning force density F_p is the pinning force per unit volume of a pinning centre, given as a product of the critical current density and the corresponding magnetic flux density: $F_p = J_c B$.

The pinning becomes most effective when the thickness of the sample, d becomes of the order of λ. For $d << \lambda$ the pinning force vanishes. A successful theory for the description of random pinning is the collective pinning theory [20], which assume that the long-range order of the vortex lattice is destroyed by the presence of the disorder, leaving a short range order over some correlation length L_c which depends on the elasticity of the lattice determined by the vortex – vortex interaction and on the disorder. Each correlated volume is assumed to be pinned independently by a total pinning force. The critical current can then be estimated from the equilibrium condition between the driving Lorentz force and the total pinning force acting on this volume. The disorder strength is parameterized by $\gamma = f_p^2 n_i \xi^2$ where f_p is the elementary pinning force for a single defect and n_i is the concentration of defects. The collective pinning length L_c is given by:

$$L_c = \left(\frac{\varepsilon_0^2 \xi^2}{\gamma} \right) \qquad (1.15)$$

where ε_o is related to the energy of a vortex line per unit length

$$\varepsilon_o = \left(\frac{\Phi_o}{4\pi\lambda} \right)^2 \qquad (1.16)$$

For weak disorder (small γ) the collective pinning length L_c is typically much larger than the coherence length ξ, $L_c >> \xi$. For $L_c \sim \xi$, the pinning should be considered as strong.

In the collective pinning theory the critical current density J_c is determined by equating the total effective pinning force $(\gamma L_c)^{1/2}$ with the lorentz force $J_c \Phi_o L_c/c$ and is given by

$$J_c \approx J_o \left(\frac{\xi}{L_c} \right)^{1/2} \qquad (1.17)$$

The regime of weak collective pinning (large $L_c >> \xi$) is characterized by a large reduction of the critical current density J_c with respect to the depairing value J_o. On the other hand, in the strong pinning regime, with $L_c \sim \xi$, the critical current density J_c achieves its maximum possible value of the depairing current J_o. This is the situation one needs for practical purposes in hard type II superconductors.

At high magnetic fields, the condensation energy decreases which leads to a corresponding decrease of J_c.

6.5 The resistive state of type II superconductor

As mentioned above, the flow of magnetic vortices under an external current leads to the generation of an electric field. This state of type II superconductor is called the reisistive state. The corresponding resistivity is called the flux-flow resistivity ρ_f and is given by the following simple expression

$$\rho_f = \frac{\Phi_o B}{c^2 \eta} \qquad (1.18)$$

Where η is the viscous drag coefficient and it is given by:

$$\eta = \frac{\Phi_o H_{c2}}{\rho_n c^2} \qquad (1.19)$$

Where ρ_n is the normal-state resistiviy of a material [21].

7. High temperature superconductivity

Since the discovery of superconductivity in 1911, the search for superconductivity with high transition temperature, above the liquid nitrogen temperature of 77K, has been one of the most challenging tasks to physicists and material scientists.

In 1986 Bednorz and Muller made a remarkable discovery, they achieved superconductivity at around 30 K in the Ba-La-Cu-O system [22]. The material they used was La_2CuO_4, in which Ba, Sr or Ca was introduced to replace some of the La atoms. Several months after the discovery of the Ba-La-Cu-O system, groups at the universities of Alabama and Houston jointly announced the discovery of superconductivity above 77 K in the Y-Ba-Cu-O (YBCO) system [23]. With the exact stoichiometry and the general structure of the superconducting phase determined. Attempts were made to replace Y by the rare-earth elements to examine their role in high-temperature superconductivity. It was found that nearly all of the rare-earth elements, including magnetic rare earths like Gd, could be substituted for Y without having a significant effect on the transition temperature. Thus a new class of superconductors, $ABa_2Cu_3O_{7-\delta}$ with A=Y, La, Nd, Sm, Eu, Gd, Ho, Er or Lu, with T_c above 90 K was discovered. There are two exceptions, the rare earth Ce and Pr. In 1988, many new compounds and classes of compound were discovered. Notable among these with the Bi-Sr-Cu-O and the Bi-Sr-Ca-Cu-O (BSCCO) compound with transition temperature up to 115 K and the Tl-Ba-Ca-Cu-O (TBCCO) compounds with transition temperature up to 125 K [24].

The family of high-T_c superconductors is very large. Despites the high T_c compounds having many different structures

presence of the cooper oxide layers.

For large-scale applications, large currents in superconducting wires and cables are required in environments where the magnetic field is strong. The advantage of high-T_c superconductors is that superconductivity is achieved above 77 K which means that they can be cooled using liquid nitrogen. High-T_c superconductors should be type II materials with extremely high H_{c2} values. Currents applications for high-T_c superconductors include wires and superconducting magnets, magnetic levitated trains, etc.

For practical applications the flux-flow regime must be avoided. Specific quantum properties of superconductors generally valid at 77 K can be used for electronic applications. Very promising is the use of high-T_c superconductors in passive microwave devices such as transmission lines and high quality resonators. The best known examples for the active devices are the Superconducting Quantum Interference Device SQUIDs and detectors based on Josephson and quasiparticle tunnelling.

High temperature superconductivity is now evolving from a research area to a commercial industry. However, the practical use of high-T_c superconductors is more difficult than was expected, and to take full advantage of superconductivity at 77 K many fundamental and technological problems remain to be solved.

7.1 Features of High-temperature superconductors

High-T_c superconductors (HTSC) are extreme type-II superconductors containing Abrikosov flux lines in a large range of applied fields between $H_{c1} \approx 0.01$ T and $H_{c2} \approx 100$ T. Apart from their high transition temperatures ($T_c \approx 90$ - 125 K), HTSC differ from conventional

superconductors by their short coherence length ξ, large magnetic penetration depth λ, and pronounced material anisotropy and layered structure.

These four properties drastically enhance the thermally activated depinning of flux lines. Small ξ reduces the pinning energy. Large λ softens the flux-lines lattice (FLL) and thus reduces the size of the correlated volume in which the FLL is pinned collectively. Thermal depinning means that the resistivity of a HTSC in a magnetic field does not completely vanish even at low current densities. The layered structure of HTSC causes two fascinating novel phenomenon: I: A flux line is now a string of two-dimensional pancake vortices in the superconducting CuO layers. These 2D vortices interact magnetically over a distance λ and by Josephson coupling between neighbouring layers. Strong coupling means that this stack of 2D vortices behaves as a usual 3D flux line. Weak coupling means (large anisotropy) means the flux line is very flexible and can evaporate into independent 2D pancake vortices. Furthermore, uncorrelated 2D vortex lattices can occur in the CuO layers, and in zero magnetic field values, spontaneous nucleation of vortex-anti-vortex pairs can cause a Kosterliz-Thouless phase transition. II: flux lines parallel to the CuO layers are "Josephson vortices" which have their core in between layers where the superconducting order is reduced or zero. In oblique applied field the vortices form kinks consisting of pancake vortices connected by Josephson vortices. All these features strongly influence the resistivity of HTSC [25].

Chapter 2

Numerical Method

In this chapter we describe our system of superconducting material with square vortex array. We present the equation of motion governing the motion of vortices. we end the chapter by discussing the numerical method used to solve the equations of motion.

1- Introduction:

In high-T_c superconductors (HTSCs), there is a total expulsion of magnetic flux up to a lower critical field H_{c1}, at fields greater than the upper critical field H_{c2} there is complete penetration of magnetic flux and the material becomes normal, and at field between H_{c1} and H_{c2} the magnetic field penetrates the HTSC in the form of quantized magnetic flux lines (vortices). The total magnetic flux that each vortex contains is exactly one quantum of magnetic flux $\Phi_0 = hc/2e = 2.07 \times 10^{-15}$ Wb, where h is Plank's constant that equals 6.62629×10^{-34} J s, and e is the charge of electron that equals 1.60219×10^{-19} C. The vortices repel each other and spread out over the entire superconductor volume forming a regular array, known as the Abrikosov vortex lattice.

In order to use the HTSCs in technology, vortices must be pined in there places. When the pinning force is equal to the maximum deriving Lorentz force the vortices will be stationary. In addition spacial inhomogeneity of the superconducting material will contribute to a finite pinning force.

At high temperature, the pinning of vortices in HTSCs was found to be fairly weak [26, 27]. Hence there have been many efforts to enhance the pinning properties in HTSCs by creating structural defects in them using energetic radiations. Irradiation by neutrons [28–32], protons

[33], electrons [34, 35], *x*-rays [36], and heavy ions [37–42] has been very successful in this respect.

General interest in lithographically-created well-defined nanostructure periodic arrays of pinning centres has now increased such that it is possible to construct samples with well defined periodic pinning structures in which the microscopic pinning parameters, such as size, depth, periodicity, and density, can be carefully controlled [26, 43–48].

Periodic pinning arrays are also of technological importance since the arrays can produce higher critical current density than in the case of an equal number of randomly placed pins [49, 50]. This enhancement of critical current density using periodic arrays has recently been demonstrated for high critical temperature (high-Tc) systems [51, 52].

Recent simulations of vortices interacting with periodic pinning arrays [52–55] or random pinning distributions [56] did not focus on the effect of size of pinning centres on the behaviour of the critical current density as function of temperature. Instead those studies have focused on the ordering states of vortex lattice at integer matching fields [53], at fractional submatching fields [54], on the multivortex states [55], and on the melting transition in a random disorder and at a fixed temperature [56]. Owing to its large impact on technological development of HTSCs, the temperature dependence of the critical current density is one of the most important aspects being studied in experimental research on HTSCs.

We have recently performed numerical calculations on the effect of pinning density and pinning strength on the critical current density as a function of temperature [56, 57]. In the present work, we extend our previous calculations to investigate the effect of the size of pinning centres on the behaviour of the critical current density in square periodic arrays of

pinning sites as the pinning strength is varied. We relate our results to theoretical, numerical, and experimental data published in several articles. [59]

2- The system:

We consider a 2D transverse slice (in the *xy*-plane) of an infinite 3D slab containing rigid vortices and columnar defects, all parallel to both the sample edge and the applied field $\mathrm{H} = H\hat{z}$. These vortices attain a uniform density n_v, allowing us to define the external field $H = n_v\Phi_0$. This model is most relevant to superconductors with periodic arrays of columnar defects or thin-film superconductors where the vortices can be approximated by 2D objects.

Figure 2.1 is a schematic plot of square pinning sites and vortices and the forces between them.

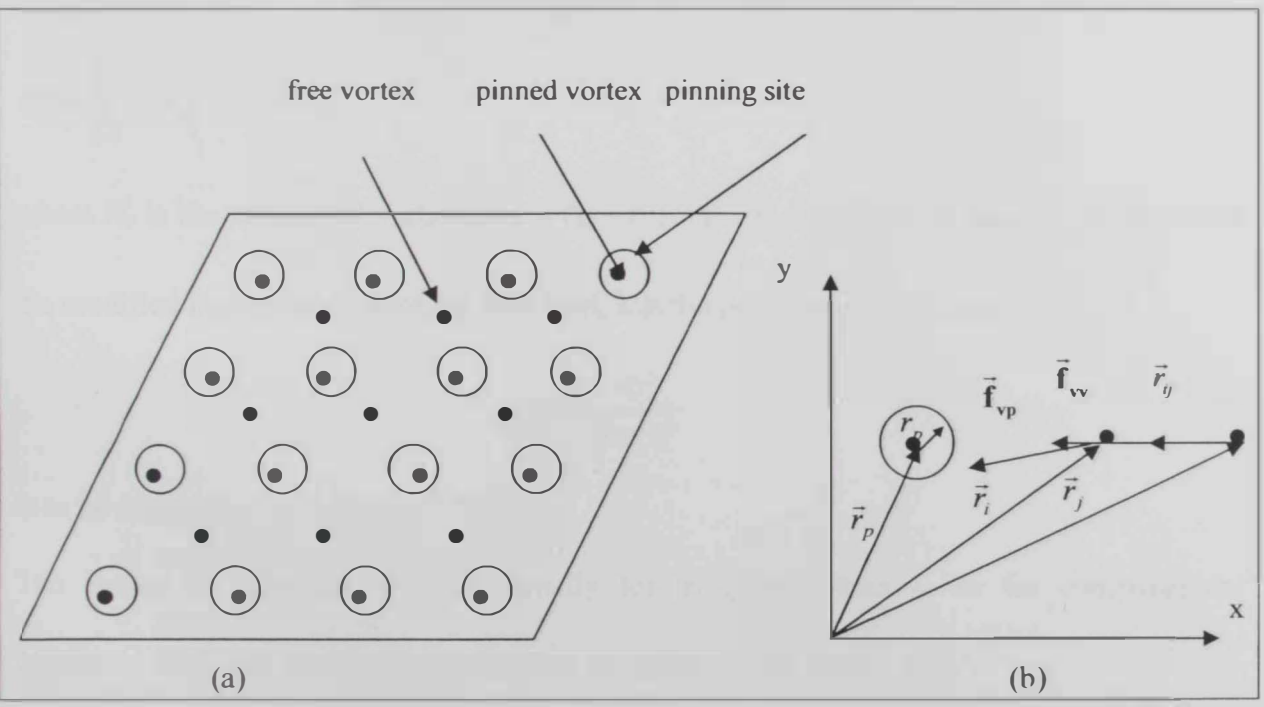

Figure 2.1: (a) Schematic plot of square pinning sites represented by circles and vortices represented by dots.(b) Vortex-vortex and vortex pin forces.

3- The equation of motion:

The over-damped equation of motion for each vortex is given by [58, 56, 57]:

$$\mathbf{f}_i^{tot} = \mathbf{f}_i^{vv} + \mathbf{f}_i^{vp} + \mathbf{f}_i^{T} + \mathbf{f}_d = \eta \mathbf{v}_i, \qquad (1)$$

where $\mathbf{f}_i^{tot}$ is the total force on vortex *i*, $\mathbf{f}_i^{vv}$ is the vortex-vortex force, $\mathbf{f}_i^{vp}$ is the vortex-pin force, $\mathbf{f}_d$ is the driving force in the *x*-direction corresponding to the Lorentz force, and $\mathbf{f}_i^{T}$ is the effective force resulting from thermal noise. The difference forces appearing in equation (1) are described in details in the following subsections:

3.1 The vortex-vortex force

The force due to the interaction of vortex *i* with other vortices $\mathbf{f}_i^{vv}$, is given by [53]:

$$\mathbf{f}_i^{vv} = \sum_{j=1}^{N_v} f_0 K_1\left(\frac{|r_i - r_j|}{\lambda}\right)\hat{r}_{ij}, \qquad (2)$$

where N_v is the number of vortices, $\hat{\mathbf{r}}_{ij} = (\mathbf{r}_i - \mathbf{r}_j)/|\mathbf{r}_i - \mathbf{r}_j|$, (shown in figure 2.1), $K_1(r/\lambda)$ is the modified Bessel function of the first kind, λ is the penetration depth, and

$$f_0 = \frac{\Phi_0^2}{8\pi^2\lambda^3} \qquad (3)$$

Is to be considered as our unit of force.

The Bessel function decays exponentially for $|\mathbf{r}|$ greater than λ, so for computational efficiency we found that the interaction can be safely cut off at 6λ [47].

In thin-film superconductors the long range vortex-vortex interaction decays as 1/r unlike in 3D bulk superconductors; however, the excellent agreement between calculated results and

experiments in thin films [31, 53] indicates that the calculated results are valid for both slabs and thin films and are general enough to be applicable to other system with repulsive particles on a periodic substrate (e.g., colloids).

3.2 The vortex-pin force

The vortex-pin force $\mathbf{f}_i^{vp}$, it is given by:

$$\mathbf{f}_i^{vp} = \sum_{k=1}^{N_p} \left(\frac{f_p}{r_p} \right) | \mathbf{r}_i - \mathbf{r}_k^{(p)} | \Theta \left(\frac{\mathbf{r}_p - | \mathbf{r}_i - \mathbf{r}_k^{(p)} |}{\lambda} \right) \hat{\mathbf{r}}_{ik}^{(p)}, \qquad (4)$$

where Θ is the Heaviside step function, f_p is the maximum pinning force, N_p is the number of pinning sites, r_p is the radius of the pinning sites, r_k is the position of the k^{th} pinning site, and $\hat{\mathbf{r}}_{ik}^{(p)} = (\mathbf{r}_i - \mathbf{r}_k^{(p)}) / | \mathbf{r}_i - \mathbf{r}_k^{(p)} |$.

vortex-pin force can be also taken as parabolic function, but we didn't take as a parabolic function we take only the Heaviside step function Θ.

3.3 The driving force

If an external current density **J** is applied to a superconductor in the mixed state it will cause the flux lines to move under the action of Lorentz force $\mathbf{F}_L$ = **J** x **B**/*c*, where $B = n\phi_0$ and n is the vortex density per unit area [26,60].

This motion of vortices produce a finite electric field **E** = -**B** x **v**/*c* along **J**, where **v** is the vortex velocity. These motions cause power dissipation in the superconductor. To prevent this dissipation, the vortices have to be pinned such that **v** = 0. In this case the driving Lorentz

force is counter acted by the pinning force f_p. Fortunately, special inhomogeneity of the superconducting material will contribute to a finite pinning force. The vortices will be stationary when the pinning force is equal to the maximum driving Lorentz force and the critical current density is thus given by $J_c = cf_p/B$ (for **J** perpendicular to **B**). This critical current density leads to the depinning of the vortices and hence to reappearance of dissipation. Dissipation-free flow is thus a matter of optimizing the pinning force f_p to give the largest J_c possible.

3.4 Effect of the temperature

The thermal fluctuations are accounted for by a stochastic term that has the properties $< f_i^T >= 0$ and $< f_i^T(t) f_j^T(t') >= 2\eta k_B T \delta(t-t')\delta_{ij}$, where f_i^T is given by $f_i^T = Af_0$, and A is the number we tune to vary T. In this manner the temperature is given by $T = 1/(2\eta k_B)(Af_0)^2 \Delta t$, where Δt is the time step used in the numerical simulation [47].

4- The numerical method:

Our system has a size of 36λ x 36λ. The pinning sites are distributed over this area in a square array with a density $n_p = 2.0/\lambda^2$. We measure all forces in units of $f_0 = \phi^2_0 /8\pi^2\lambda^3$, fields in units of ϕ_0/λ^2, lengths in units of λ, temperature in units of f_0/k_B, and the velocity in units of f_0/η. Furthermore we take $f_0 = k_B = \eta = 1$.

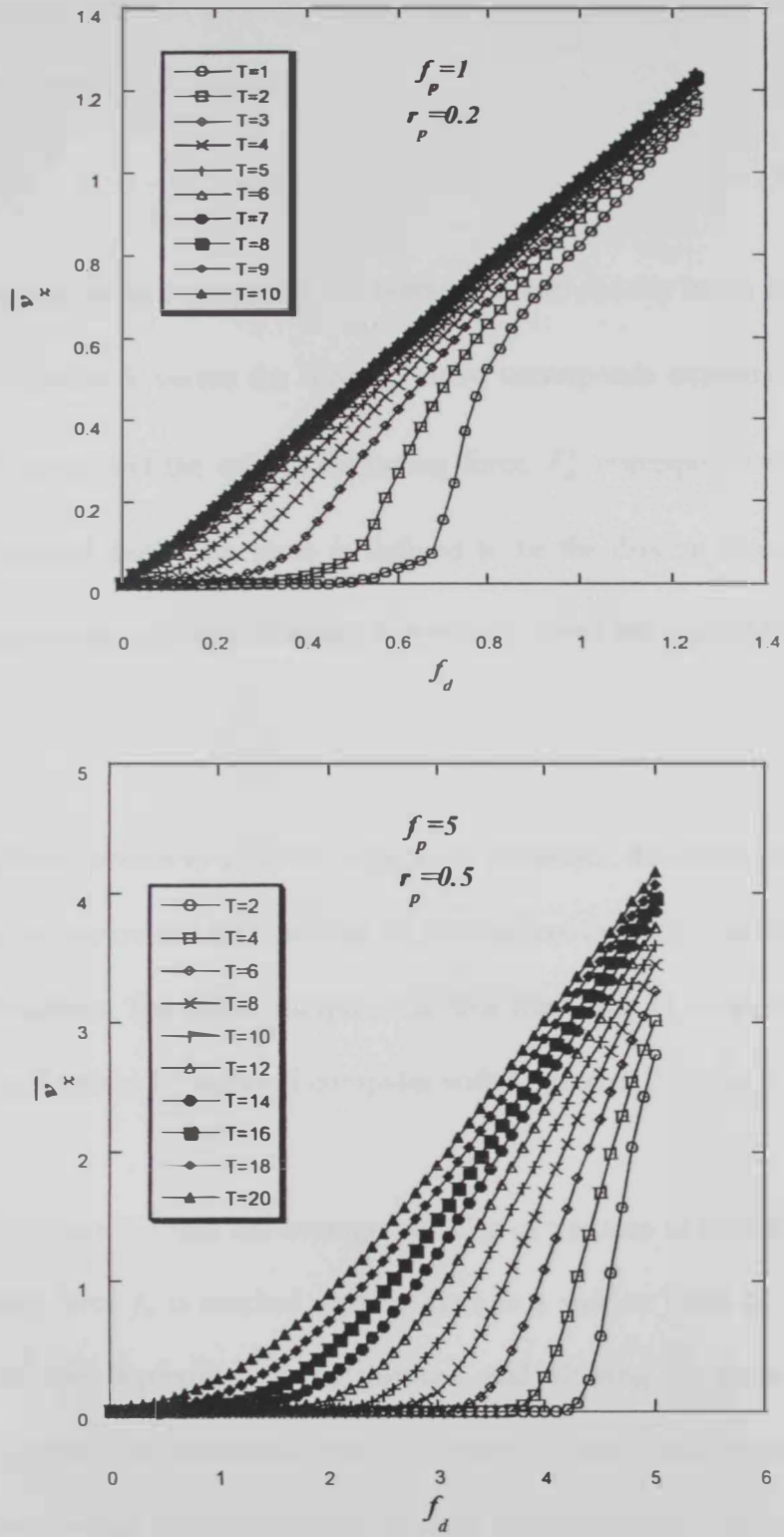

Figure 2.2: The average velocity $\bar{v}_x$ vs. the driving force f_d at different temperatures. $\bar{v}_x$ is in units of f_0/η and f_d is in units of f_0.

Initially, we place the vortices of density $n_v = 0.75/\lambda^2$ in a perfect square lattice, then slowly increase a spatially uniform driving force f_d from zero to a maximum value and measure the average velocity over all N_v vortices:

$$\bar{v}_x = \frac{1}{N_v}\sum_{i=1}^{N_v} \mathbf{v}_i \cdot \hat{\mathbf{x}} \qquad (5)$$

For each drive increment we measure the average vortex velocity in the direction of drive, $\bar{v}_x$. The average velocity $\bar{v}_x$ versus the force f_d curve corresponds experimentally to a voltage-current, V (I), curve and the critical depinning force F_d^c corresponds to the critical current density. The critical depinning force is defined to be the driving force value at which $\bar{v}_x$ exhibits a sharp jump and thus marking a transition from the pinned to the moving vortex phase.

We used the Euler method to solve the equations of motion. The time step used is $\Delta t = 0.02$. We found that the maximum time needed for the vortices to reach a steady state is 2×10^4 for all of our calculations. The actual computation time was about 11 hours for each curve of Fig. 2 performed on Pentium IV personal computer with a speed of 2.2 Ghz.

We can see in figure 2.2 that the average velocity of vortices is almost zero until a critical value of driving force f_d is reached where there is a sudden jump in the average velocity corresponds to the depinning of all vortices and flowing in same direction. And as temperature increase the depinning shift to lower f_d value, also we can see that at high temperature the average velocity increase linearly with f_d, and as f_d get very large the curves converge and linear regime is attained

Chapter 3

Results and discussion

1- Introduction

In this chapter, we present the results that we have obtained through the simulations of driven vortices to study the effect of the pinning size on the critical current density.

The system we consider is a two-dimensional transverse slice (in the xy plane) superconductor, which contains a fixed number of vortices $N_v = 961$, and a fixed number of pinning sites, $N_p = 2601$. These pinning sites are ordered in square lattice of size $36\lambda x36\lambda$. This corresponds to a density $n_p=2/\lambda^2$, and $n_v = 0.75/\lambda^2$.

We have simulated the dynamics of the vortices in this system starting from a initial state where all the vortices are pinned. By applying a force F and tuning on the temperature vortices start to move.

The average velocity of all vortices is computed as a function of time. Once the average velocity reaches a steady value, the values of the velocity and the corresponding driving force are recorded. Finally a curve, such as figure 3.1 represented the average velocity versus the driving force is obtained.

Physically, the driving force represents the Lorentz force due to an applied current and the average velocity is proportional to the potential difference.

This kind of simulation has been carried out extensively with different parameters. Since in this study we are interested in the effect of the pinning size on the critical current density, we varied the pinning strength f_p and the pinning size r_p, with $f_p= (1, 3, 5)f_o$ and $r_p = (0.2\text{-}0.6)\lambda$, with a step of 0.1λ. when we increasing the pinning size, we made sure that they do not overlap [33,34,54].

2- The vortex average velocity $\bar{v}_x$ versus the driving force f_d

In molecular dynamic simulations, we have used the over-damped equation for each vortex in the system .

We have calculated the average velocity $\bar{v}_x$ for all the vortices in the system as the driving force is increased. Fig 3.1 represents the steady state average velocity $\bar{v}_x$ versus the driving force f_d for $f_p = f_o$, $r_p = 0.2\ \lambda$, and for 2 temperature $T_1 = 1$, $T_2 = 4$ (where the temperature is measured in units of f_0/k_B).

The curves clearly show 2 different regions for each temperature. The first region has very low average velocity, which corresponds to the system of pinned vortices, and the second region corresponds to unpinned vortices where the average velocity increases linearly with the driving force.

In between, there is a critical region, where the value of the driving force for which the average velocity $\bar{v}_x$ has a sudden jump corresponds to the critical value F_d^c of the driving force, that is the maximum force before the vortices get unpinned.

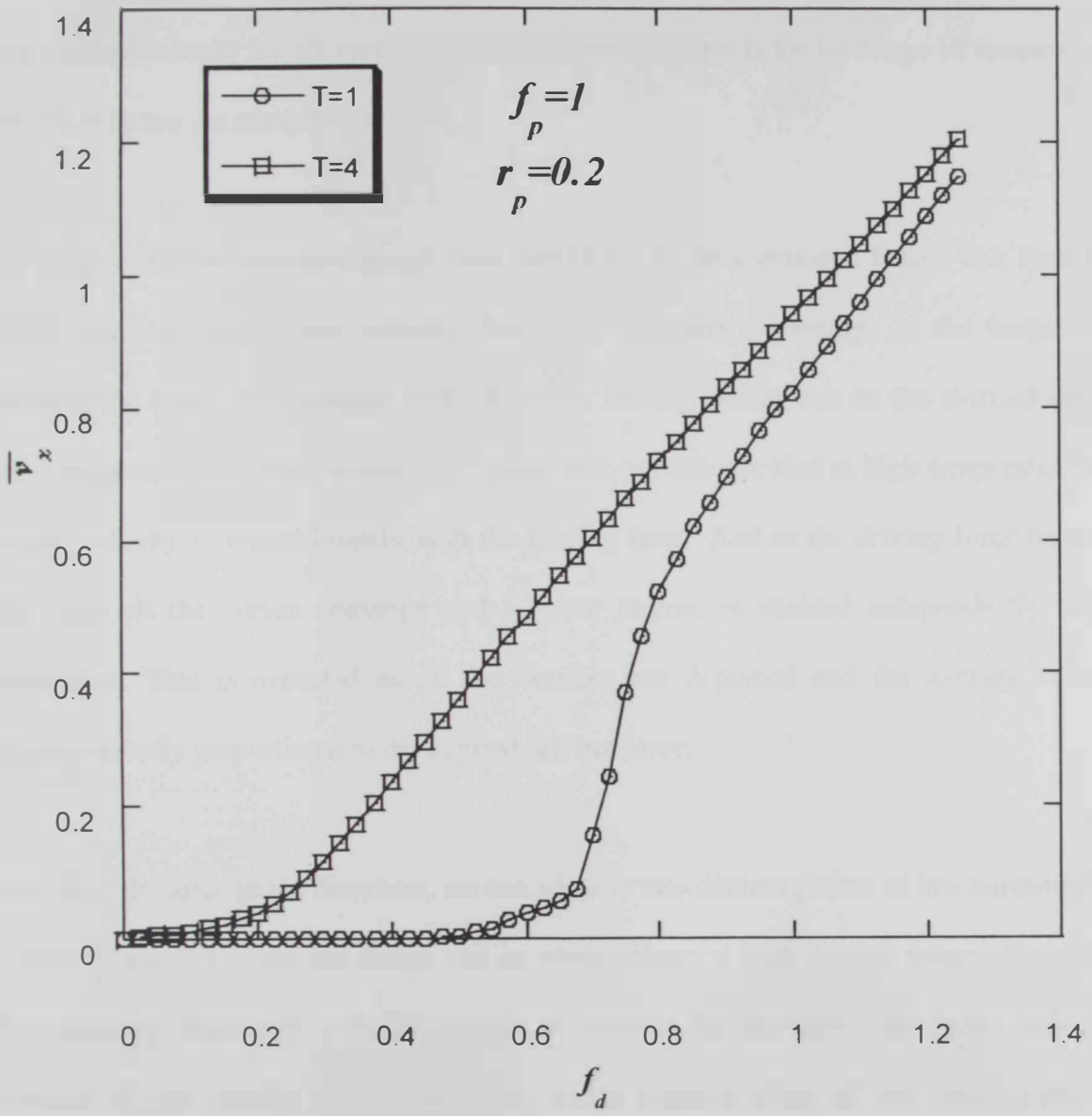

Figure 3.1: The average velocity $\bar{v}_x$ vs. the driving force f_p at two different temperatures.

All the fifteen cases, corresponding to the three values of f_p and the five values of r_p, are represented in figs. 3.2-3.4.

For each set of parameters, such as f_p=1 and r_p = 0.2 shown in fig. 3.2a, we plot the steady state average velocity for all vortices versus the driving force f_d for the range of temperatures T=1-10, with temperature step of 1.

The general observation one can see from figs (3.2-3.4), as mentioned before that there is a sudden jump in the average velocity due to the vortices depinning, as the temperature increases the onset of depinning shifts to lower driving forces due to the thermal energy which suppresses the effect of pinning forces, also we can see that at high temperatures the average velocity increases linearly with the driving force. And as the driving force becomes very large all the curves converge and a linear regime is attained independently of the temperature. This is expected as all the vortices are depinned and the average velocity becomes directly proportional to the applied driving force.

From these dynamic phase diagrams, we can identify two distinct phases at low temperatures; a plastic phase at low driving forces and an elastic phase at high driving forces. The plastic phase appears when only a small number of vortices are depinned and move under the influence of the driving force. The elastic phase appears when all the vortices become depinned and flow collectively in one direction, giving a sharp rise in the average velocity. The transition from plastic to elastic phase is smeared out as temperature increases and disappears at high temperatures, where we see only an elastic phase.

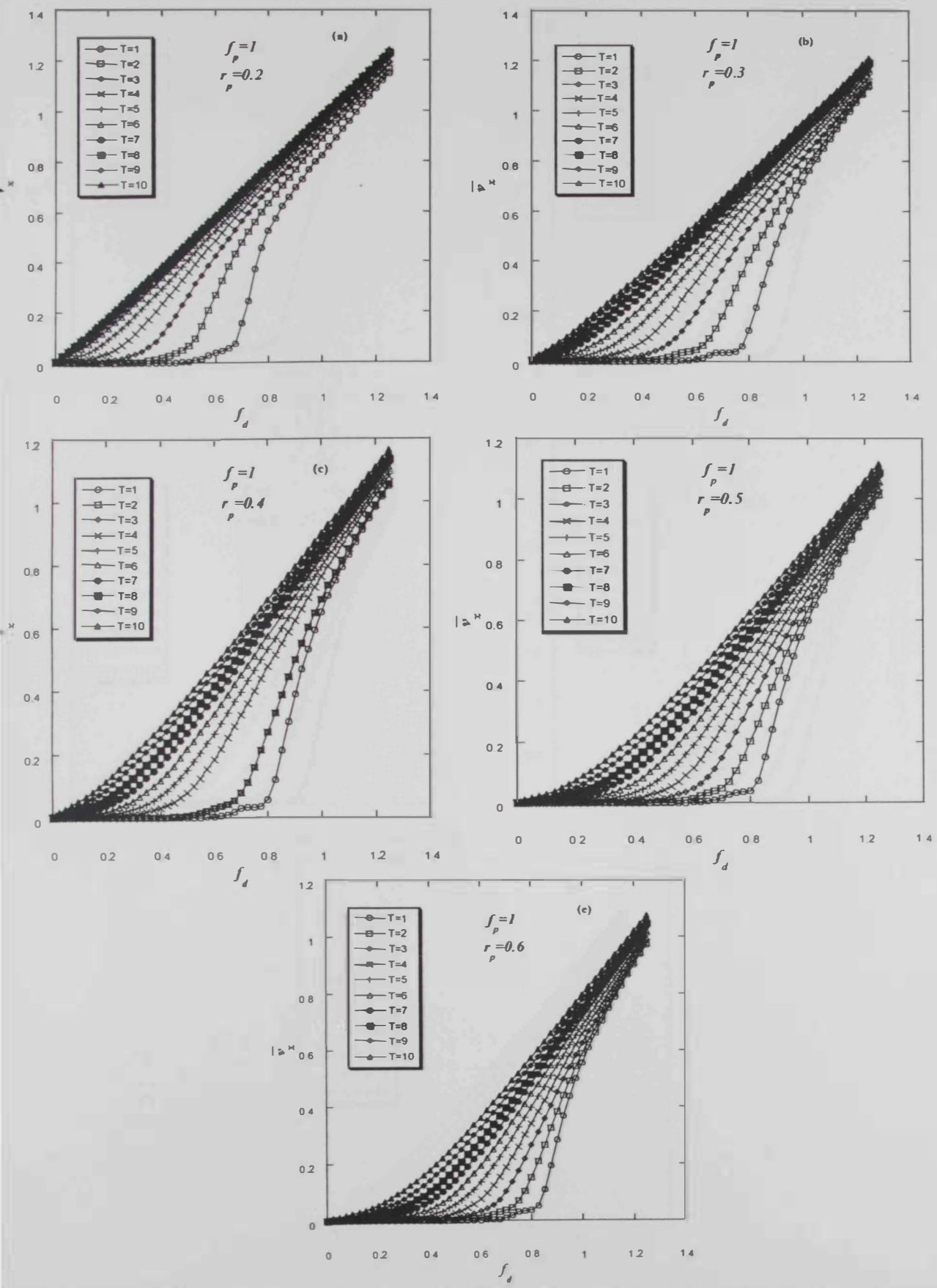

Figure 3.2: The average velocity $\bar{v}_x$ vs. the driving force f_d for $f_p=1$, for different r_p and different temperatures. $\bar{v}_x$ is in unit of f_o/η and f_d is in unit of f_o.

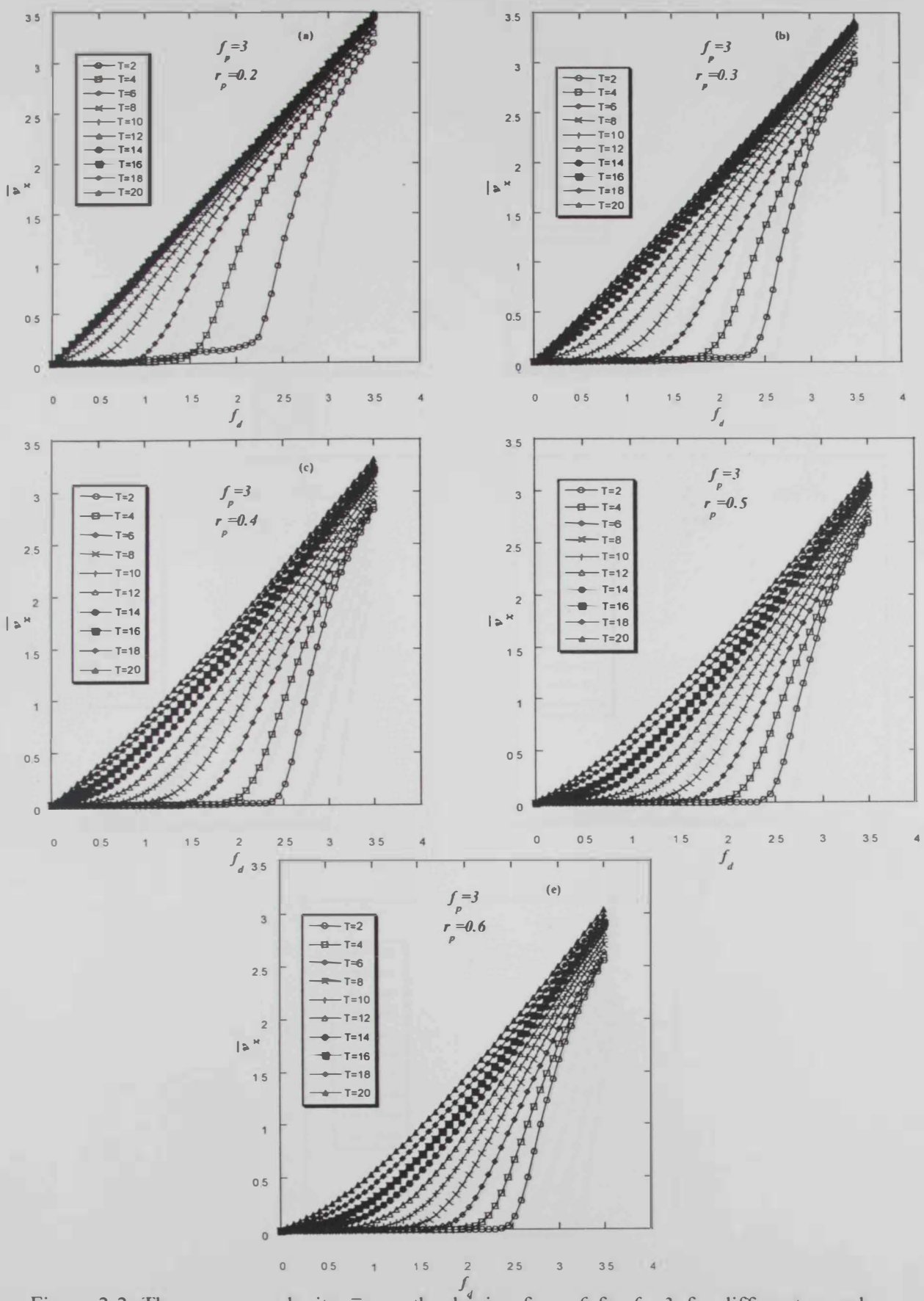

Figure 3.3: The average velocity $\bar{v}_x$ vs. the driving force f_d for $f_p=3$, for different r_p and different temperatures. Units here is the same as mentioned in figure 3.2

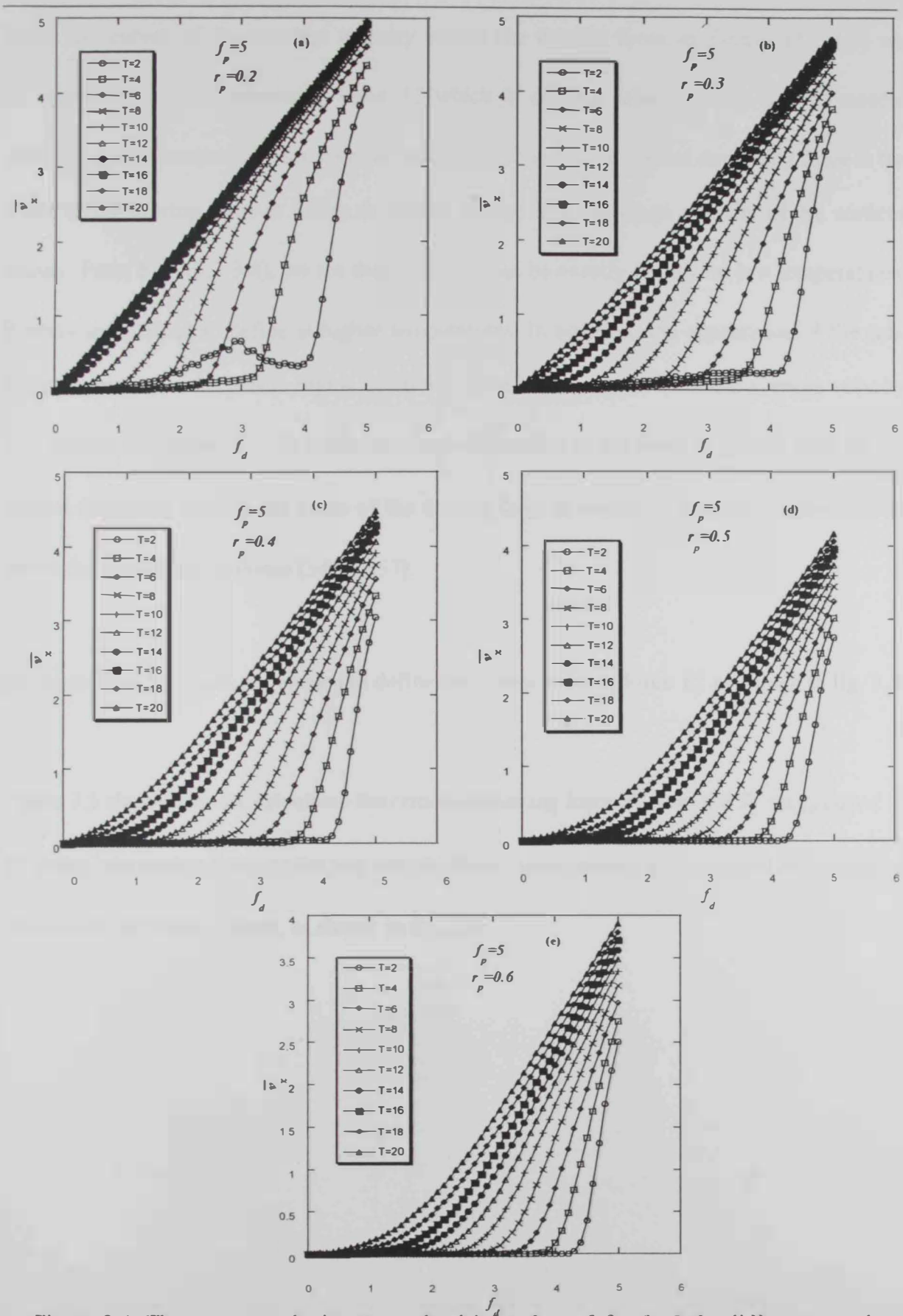

Figure 3.4: The average velocity $\bar{v}_x$ vs. the driving force f_d for f_p=5, for different r_p and different temperatures. Units here is the same as mentioned in figure 3.2

From the curves of the average velocity versus the driving force in figures (3.2-3.4) we calculated the critical depinning force F_d^c (which is directly related to the critical current density) at each temperature for specific values of r_p and f_p. The critical depinning force is the value of the driving force at which an abrupt change in the average velocity of the vortices occurs. From Figs (3.2-3.4), we see that while F_d^c can be exactly defined at low temperatures, it becomes difficult to define at higher temperatures. In addition, the appearance of the sub-ohmic behavior in the plastic region prohibits using a constant value of the average velocity as a criterion to define F_d^c . To overcome these difficulties of the suitable criteria used for the critical depinning force is the value of the driving force at which $\bar{v}_x$ reaches a value of 0.03 above the sub-ohmic response [54, 56, 57].

For a practical purposes, we chosen to define the critical driving force F_d^c as shown in fig. 3.5.

Figure 3.5 shows how we calculated the critical depinning force F_d^c from the $\bar{v}_x$ vs. f_p curve. F_d^c is the intersection between the two straight lines corresponding to the pinned and unpinned regimes of the vortex system, as shown in fig. 3.5.

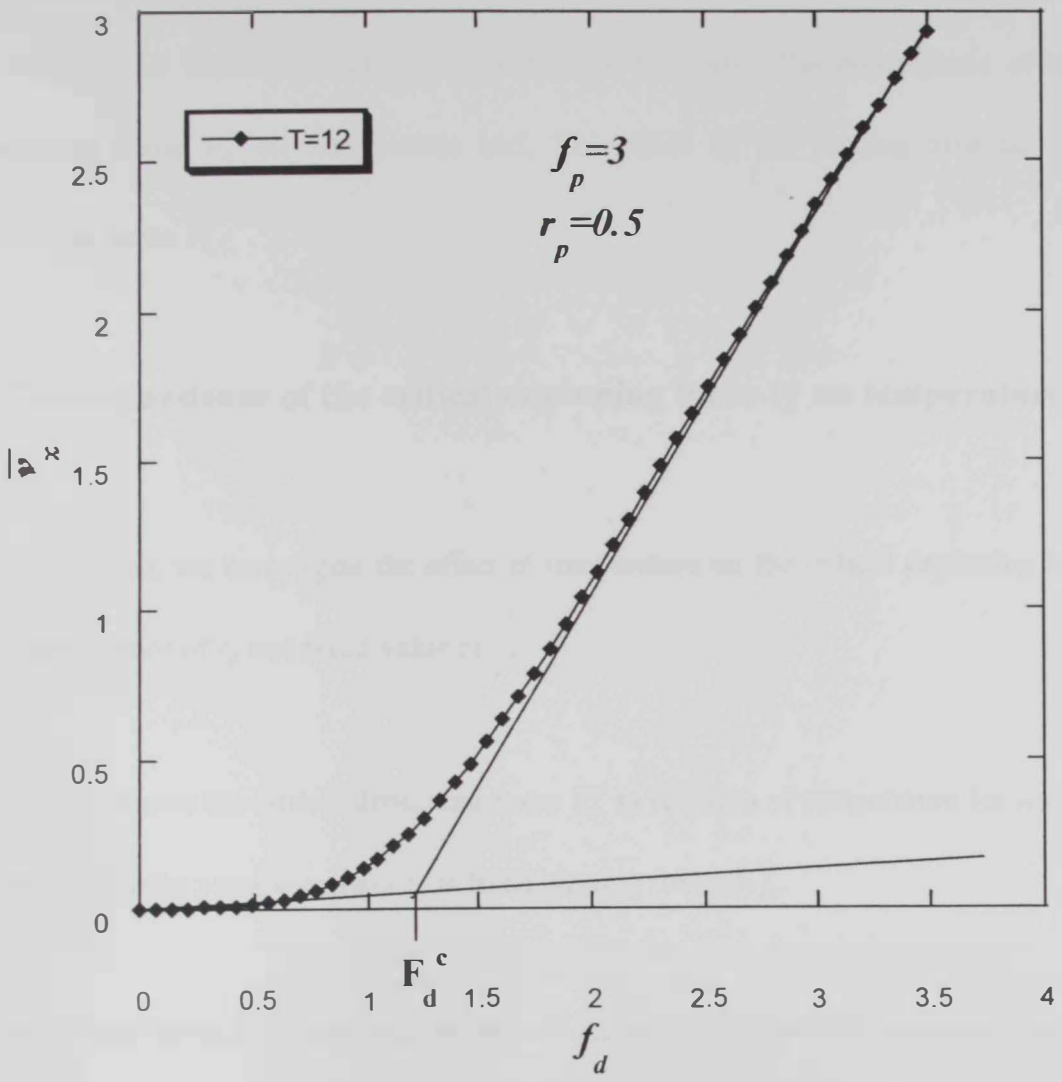

Figure 3.5: Calculation of F_d^c from the $\bar{v}_x$ vs. f_p curve

We calculated F_d^c for each temperature for each set of values of r_p and f_p. Once F_d^c was defined for all these parameters, we were able to study: The dependence of the critical depinning force F_d^c on temperature and, The effect of the pinning size on the critical depinning force F_d^c.

3. The dependence of the critical depinning force F_d^c on temperature:

In this section, we investigate the effect of temperature on the critical depinning force F_d^c for different values of r_p and fixed value of f_p.

Figure 3.6 shows the critical depinning force F_d^c as function of temperature for several values of the size of the pinning centers r_p at fixed pinning strength f_p.

It can be seen from this figure that the rate of decrease of the critical depinning force becomes faster as r_p decreases. The slowest rate of decrease of F_d^c as function of temperature occurs for the largest r_p values for all values of f_p. For $f_p = 1$, F_d^c decreases almost linearly with temperature for $r_p = 0.6$. This behavior of F_d^c as function of temperature is supported theoretically [61], where it was suggested that vortex pinning at low temperatures is predominantly produced by point defects while at high temperatures it is produced by extended defects. This was also observed experimentally [27], where a contrasting behavior of the critical current density as function of temperature in $YBa_2Cu_3O_{7-\delta}$ and $Ba_{0.57}K_{0.43}BiO_3$ polycrystalline samples was found. In $YBa_2Cu_3O_{7-\delta}$ samples, J_c was found to decrease fast at low temperatures and slows down as the temperature is increased. In $YBa_2Cu_3O_{7-\delta}$ samples, J_c

was found to decrease slowly (almost linearly) at all temperatures. The sharp decrease of J_c as the temperature increases in $YBa_2Cu_3O_{7-\delta}$ was attributed to the oxygen vacancies, which is commonly present in such samples, whereas they are essentially absent in $Ba_{0.57}K_{0.43}BiO_3$ samples. The results of our numerical calculations provide a firm and solid support to the experimental and theoretical results. Pinning centers with small r_p behave as point-like defects so they become less important in pinning vortices at high temperatures. Whereas pinning centers with large r_p behave as extended defects, which play a significant role in pinning vortices at all temperatures. Similar behavior of F_d^c versus temperature is also seen in Fig. 3.6b and Fig. 3.6c for different values of pinning strength, f_p.

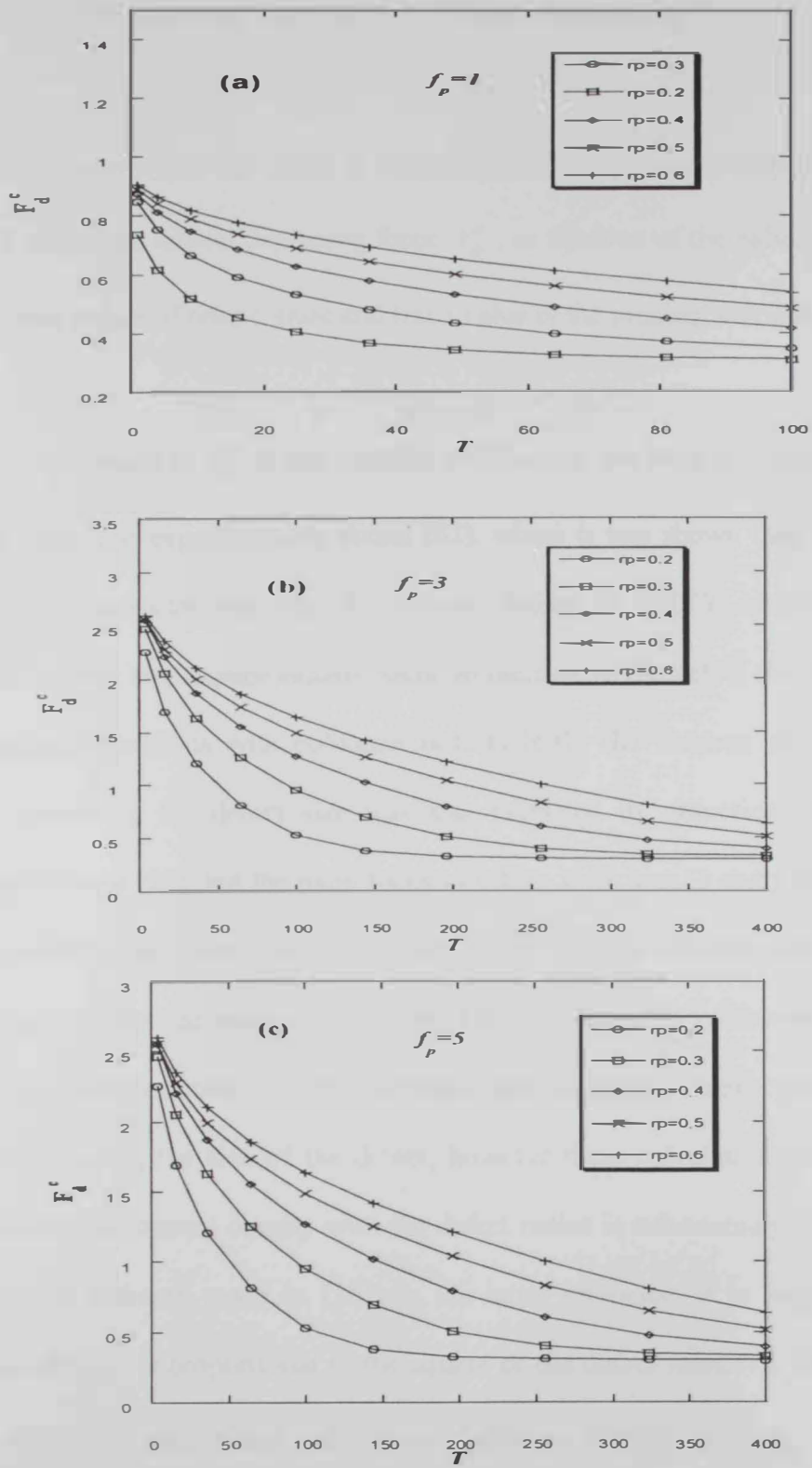

Figure 3.6: The critical depinning force F_d^c as a function of temperature for several values of the radius of the pinning center r_p and pinning strength f_p. F_d^c and f_p are in unit of f_o and T is in unit of $\lambda f_o/K_B$

4. The effect of the pinning size on the critical depinning force F_d^c

In this section, we investigate the effect of the pining radius r_p on the critical depinning force F_d^c, figure 3.7 shows the critical depinning force, F_d^c , as function of the radius of the pinning center, for several values of temperature and fixed value of the pinning strength f_p.

It is seen that the values of F_d^c at any specific temperature are large for large values of r_p. These results were also experimentally found [62], where it was shown that vortex pinning was improved by increasing the size of columnar defects in *BSCCO* single crystals. The critical current density was experimentally found to increase as the defect size increases in an array of Josephson junctions with columnar defects [63]. The increase of critical current density with increasing the defect size was also predicted by numerical calculations on periodic array of loops [55], but the main focus of others work was to study the multi-vortex states configurations and their calculations were done only at absolute zero temperature. Using numerical calculations based on Ginzburg-Landau Theory on 2-Dimensional model of extreme type-II superconductor [64] it was found that the critical current density increases linearly with increasing the size of the defect, however these calculations suggest that the increase in the critical current density with the defect radius is substantially smaller than the phenomenological estimate made in [26]. In the latter reference, it is suggested that the critical current density is proportional to the square of the defect radius r_p. We find a linear dependence of F_d^c on r_p only at high temperatures while no dependence on r_p is found at any temperature. In Figs. 3.7 and 3.8, we notice that at high temperatures, F_d^c increases almost linearly with r_p for all f_p values. As the temperature decreases, F_d^c approaches saturation at large r_p values. This saturation appears sooner at low temperatures, indicating that the

increase in the size of the defect ceases to enhance the critical current density. This puts an upper limit on the usefulness of the size of the defect in enhancing the critical current density, while at high temperatures, this role is still significant. Our simulations are made for several values of temperature ranging from very low to high temperatures. Hence, our calculation allow a more detailed and qualitative and quantitative study of the dependence of critical depinning force on the size of the pinning centers as a function of temperature and pinning strength.

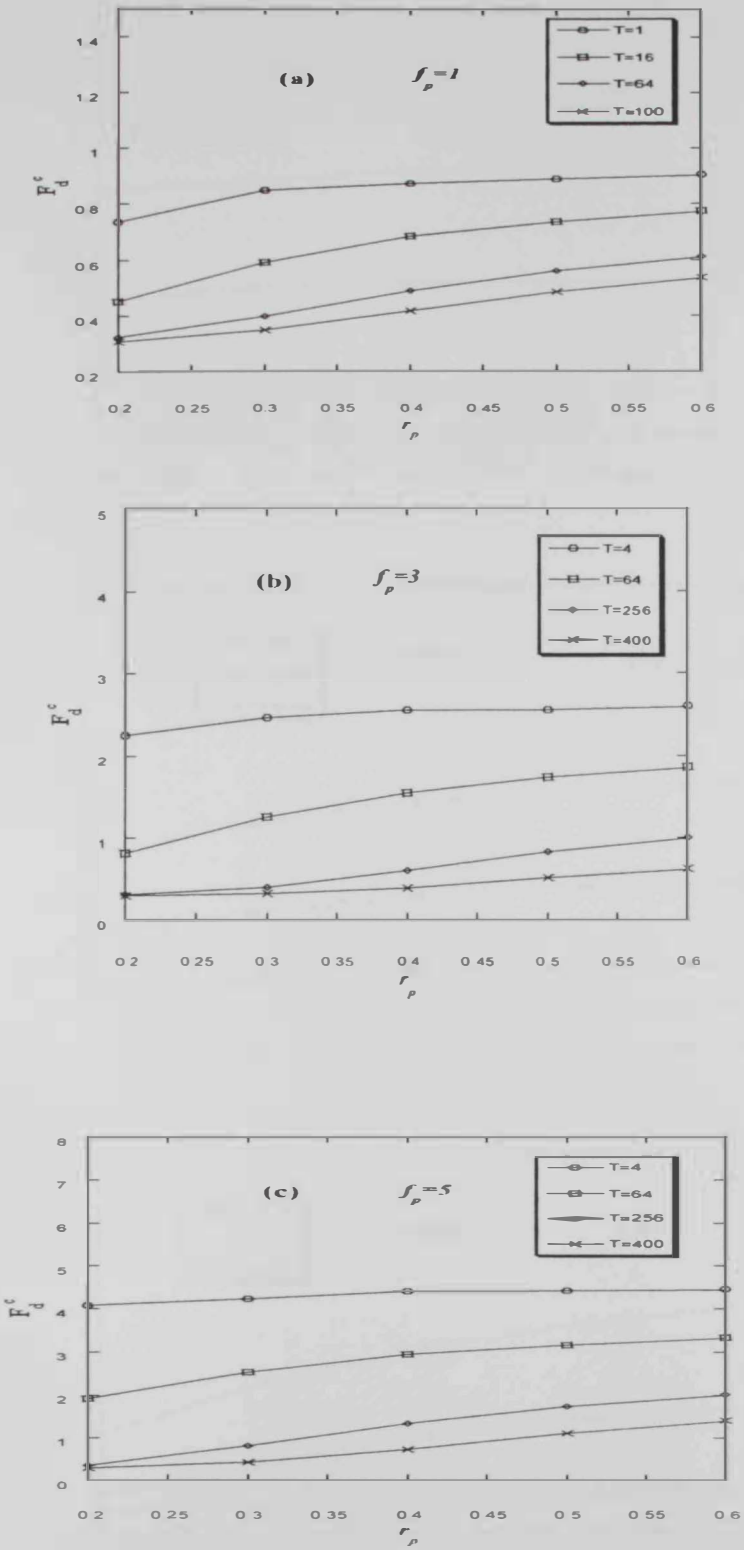

Figure 3.7: The critical depinning force F_d^c as a function of the radius of the pinning center r_p. the pinning strength f_p is fixed for all curves in the sub figures. Units here is the same as mentioned in figure 3.6

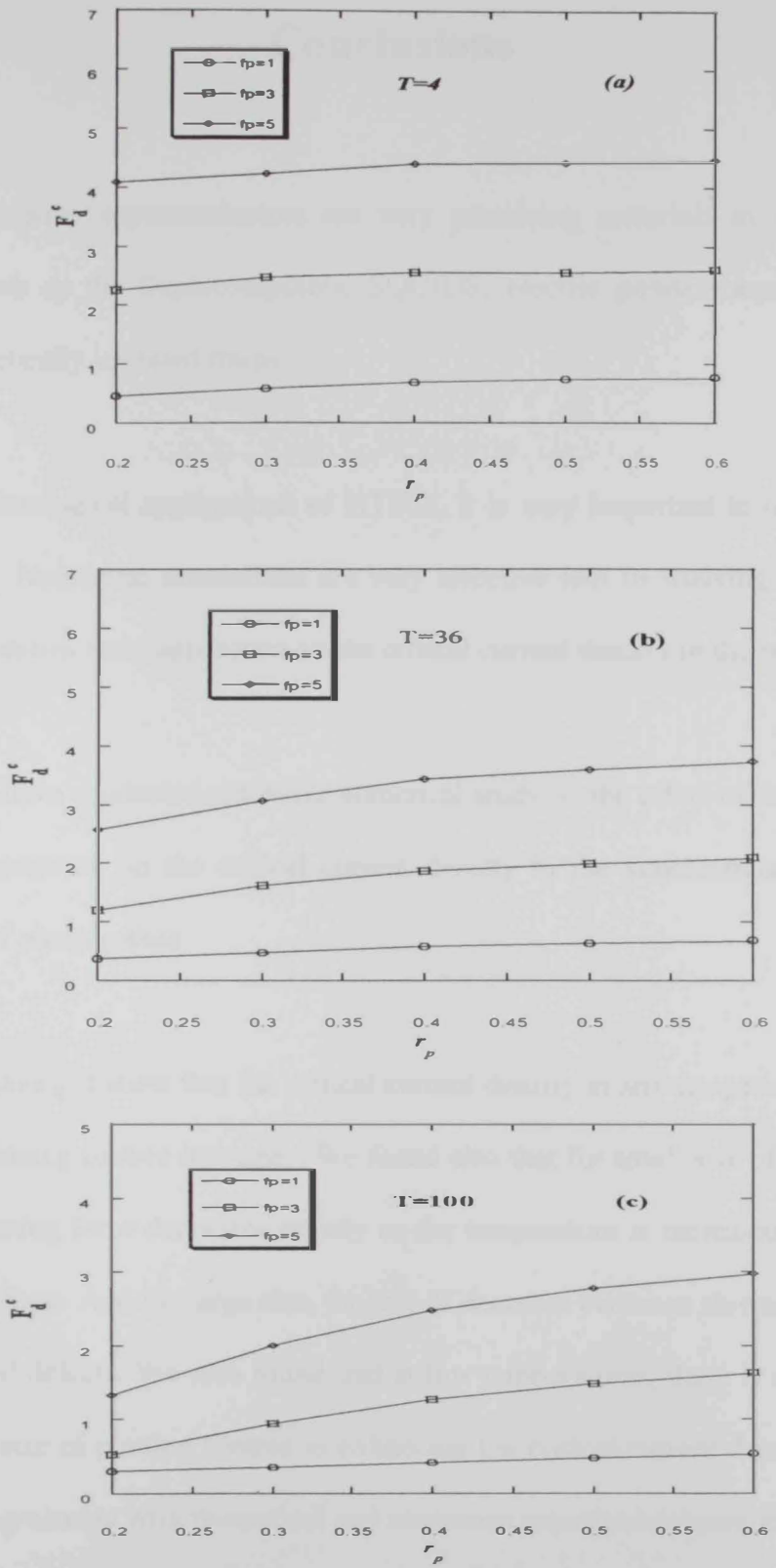

Figure 3.8: The critical depinning force F_d^c as a function of the radius of the pinning center r_p. the temperature is fixed for all curves in the sub figures. Units here is the same as mentioned in figure 3.6.

Conclusions

The high temperature superconductors are very promising materials in a wide range of applications, such as the Supercomputers, SQUIDS, electric power transmission, motors, MRI, and magnetically levitated trains.

For most of technological applications of HTSCs, it is very important to have high critical current density. Numerical simulations are very effective tool in studying the effect of the size of pinning centres and temperature on the critical current density in the superconductor.

In this thesis we have conducted extensive numerical study on the effect of the size of pinning centres and temperature on the critical current density in the superconductor with square periodic arrays of pinning sites.

The results we have got show that the critical current density at any temperature increases as the size of the pinning centres increases. We found also that for small size of pinning centres, the critical depinning force decreases rapidly as the temperature is increased, resembling the effect of point defects. And for large size, the rate of decrease becomes slower, resembling the effect of extended defects. We also found that at low temperatures, there is an upper limit to the effect of the size of pinning centres in enhancing the critical current density. Our results are in excellent agreement with theoretical and numerous experimental results.

From our results one can see that high temperature superconductors can be useful in technological application if we can increases the size of the pinning centres.

References

[1] Kamerlingh Onnes H 1991 *Lieden Commun.* 120b, 122b, 124c

[2] Meissner W and Ochsenfeld R 1933 *Naturwissenschaf*ten **21** 787

[3] Doll R and Nabauer M 1961 *phys. Rev. Lett* 7 51

[4] Josephson B D 1962 *Phys. Lett.* 1 251

[5] Myers, H.P. 1990. Introductory solid state physics. Taylor & Francis Inc.: London.

[6] Serway, R. A. 1990. Physics for scientists and engineers. 3rd ed., Sunders College Publishing: Philadelphia.

[7] Buckel, Werner. 1991. Superconductivity fundamentals and applications. VCH Puplishers Inc.: New York.

[8] Brewer, D. F., March, N. H., and Parrinello, M. 1982. Collective effects in solid and liquids. Adam Hilger Ltd: Bristol.

[9] Ashcroft, N. W., and Mermin, N. D. 1979. Solid state physics. Holt, Rinehart and Winston: Phildelphia

[10] Van Duzer, T., and Turner, C. W. 1981. Principles of superconductive devices and circuits. Elsevier North Holland, Inc.: New York.

[11] Robertson, B. C. 1981. Modern physics for applied science. John Wiley & sons Inc.: NewYork.

[12] Kittle, C. 1981. Quantum Theory of solids. John Wiley & sons Inc.: New York.

[13] De Gennes, P. G. 1989. Superconductivity of metals and alloys. Addison Wesley Publishing Co., Inc: New York.

[14] Tinkham, Michael. 1975. Introduction to superconductivity. McGraw-Hill, Inc.: Japan

[15] Shubnikov L W, Khotkevich W I, Shepelev JD, and Ryabinin J N 1937 *Sov. Phys-JETP* 7 221

[16] Trauble H and Essmann V 1967 *Phys. Lett.* **24A** 526

[17] Hu C R 1972 *Phys.Rev.* B **6** 1756

[18] Abrikosov A A 1952 *Dokl. Acad. Nauk.* **86** 489

[19] De Gennes P G 1966 *Superconductivity of Metals and Alloys* (New Yourk: Benjamin)

[20] Larkin A I and Ovchinnikov Yu N 1979 J. *Low Temp. Phys.* **34** 409

[21] Bardeen J and Stephen M J 1965 *Phys. Rev.* **140** 1197A

[22] Bednorz J G and Mullar K A 1986 *Z. Phys. B* **64** 189

[23] Wu M K, Ashburn J R. Torng C J, Hor P H, Meng R L, Gao L, Huag Z J, Wang Y Q and Chu C W 1987 *Phys. Rev. Lett.* **58** 908

[24] Zhao Z X et al 1987 Kexue Tongbao **32** 522

[25] E. H. Brandt, CHINESE JOURNAL OF PHYSICS , VOL. 31, NO. 6-11 (December 1993)

[26] C. Reichhardt, N. Gronbech-Jensen, Phys. Rev. B 63, 054510 (2001).

[27] G. Blatter, et al., Rev. Mod. Phys.66, 1125 (1994).

[28] I.M. Obaidat, H.P. Goeckner, J.S. Kouvel. Physica C 291, 8 (1997).

[29] J.S. Umezawa, G.W. Crabtree, J.Z. Liu, H.W. Weber, W.K. Kwok, L.H. Nunez, T.J. Moran. C.H. Sowers, H. Claus. Phys.Rev. B 36, 7151 (1987).

[30] J.R. Cost, J.O. Willis, J.D. Thompson, D.E. Peterson. Phys. Rev. B 37, 1563 (1988).

[31] R.B. vanDover, E.M. Gyorgy, L.F. Schneemeyer, J.W. Mitchell, K.V. Rao, Puzniak, J.V. Waszczak. Nature 342, 55 (1989).

[32] B.M. Vlcek, M.C. Frischherz, S. Fleshler, U. Welp, J.Z. Liu, J. Downey, K.G. Vandervoort, G.W. Crabtree, M.A. Kirk, J. Giapintzakis, J. Farmer. Phys. Rev. B 46, 6441 (1992).

[33] B.M. Vlcek, H.K. Viswananthan, M.C. Frischherz, S. Fleshler, K. Vandervoort, J. Downey, U. Welp, M.A. Kirk, G.W. Crabtree. Phys. Rev. B 48, 4067 (1993).

[34] L. Civale, A.D. Marwick, M.W. McElfresh, T.K. Worthington, A.P. Malozemoff, F.H. Holtzberg, M.A. Kirk. Phys. Rev. Lett. 65, 1164 (1991).

[35] M. Konczykowski, Physica A 168, 291 (1990).

[36] J. Giapintzakis, W.C. Lee, J.P. Rice, D.M. Ginsberg, I.M. Robertson, M.A. Kirk, R. Wheeler. Phys. Rev. B 45, 10677(1992).

[37] M.K. Hasan, B.A. Albiss, I.M. Obaidat, S.J. Park, J.S. Kouvel. Physica C 336, 75(2000).

[38] B.A. Albiss, H. Ozkan, H. Bocuk, N.M. Gasanly, I. Ercan. Superlattices and Microstructures, Vol. 21, Suppl. A, 1997.

[39] L. Civale, A.D. Marwick, T.K. Worthington, M.A. Kirk, J.R. Thompson, L. Krusin-Elbaum, Y.R. Sun, J.R. Clem, F. Holtzberg. Phys. Rev. Lett. 67, 648 (1991).

[40] W. Gerhauser, G. Ries, H.W. Neumuller. W. Schmit, O. Eibl, G. Samann-Ischenko, S. Kaumunzer. Phys. Rev. Lett. 68, 879 (1992).

[41] M.Xu, J.E. Ostenson, D.K. Finnemore, M.J. Kramer, J.A. Fendrich, J.D. Hettinger, U. Welp, G.W. Crabtree, B. Dabrowski, K. Zhang. Phys. Rev. B 53, 5815 (1996).

[42] J. Wiesner, C. Tracholt, J.G. Wen, H.W. Zandbergen, G. Wirth. H. Fuess. Physica C 268, 161 (1996).

[43] M. Baert et al., Phys. Rev. Lett. 74, 3269 (1995).

[44] E. Rosseel et al., Phys. Rev. B 53, R2983 (1996).

[45] V.V. Moshchalkov et al., ibid. 7385 (1996).

[46] J.Y. Lin et al., ibid. R 12 714 (1996).

[47] K. Harada, O. Kamimura, H. Kasai, T. Matsuda, and A. Tonomura, Science 274, 1167 (1996).

[48] T. Matsuda, K. Harada, H. Kasai, A. Tonomura, O. Kamimura, and V.V. Moshchalkov, Science 271, 1393 (1996).

[49] C. Reichhardt, C.J. Olson, J. Groth, S. Field, and F. Nori, Phys. Rev. B 53, R8898 (1996).

[50] C. Reichhardt, J. Groth, C.J. Olson, S. Field, and F. Nori, Phys. Rev. B 54, 16108 (1996).

[51] J.Y. Lin et al., Phys. Rev. B 54, R12 717 (1996).

[52] A. Castellanos, R. Wordenweber, G. Ockenfuss, A. v.d. Hart, and K. Keck, Appl. Phys. Lett. 71, 962 (1997).

[53] C. Reichhardt, C.J. Olson, and F. Nori, Phys. Rev. B 57, 7937 (1998).

[54] C. Reichhardt, N. Gronbech-Jensen, Phys. Rev. B 63, 054510 (2001).

[55] C. Reichhardt, Niels Gronbech-Jensen, Phys. Rev. Lett. 85, 2372 (2000).

[56] B. Y. Zhu, D. Y. Xing, Jinming Dong, and B. R. Zhao, Physica C 311, 140(1999).

[57] I. M. Obaidat, U. Al Khawaja, and M. Benkraouda, Supercond. Sci. Technol. 18, 1380 (2005).

[58] M. Benkraouda, I. Obaidat, and U. Al-Khawaja, to appear in Physica C.

[59] U. Al-Khawaja, M. Benkraouda, I. Obaidat, and S. Alneaimi, Physica C 442, 1-8 (2006)

[60] 1. M. Tinkham, *Introduction to Superconductivity*, McGraw-Hill, Chapter 5, 1996.

[61] T. Hwa, D. R. Nelson and V. M. Vinkur, Phys. Rev. B 48, 1167 (1993).

[62] S. Hebert, V. Hardly, M. Hervieu, G. Villard, Ch. Simon, and J. Provost, Nucl. Inst. and Meth. in Phys. Res. B 146, 545 (1998).

[63] D. Bhattacharya, A. Pandey, and R. G. Sharma, Physica C 341-348, 1205 (2000).

[64] S. M. Maurer, M-C. Yeh and T. A. Tomberllo, J. Phys. Condensed Matter 10, 7429 (1998).

أثر حجم المعوقات على كثافة التيار الحرج في المواد فائقة الموصلية ذوات درجة الحرارة الحرجة العالية

الخلاصة

تعتبر المواد فائقة الموصلية ذوات درجة الحرارة الحرجة العالية من المواد الهامة في الكثير من التطبيقات، مثل أجهزة الحاسوب السريعة و ذات السعة التخزينية الكبيرة ، و موصلات الطاقة الكهربائية و التصوير بالرنين المغناطيسي.

ونظرا لأهمية هذه المواد في التطبيقات التكنولوجية فإن من المهم لهذه المواد أن تكون ذات كثافة تيار حرج عالية. و تعتبر التشبيهات الرقمية من أهم الوسائل لدراسة تأثير حجم المعوقات و الحرارة على كثافة التيار الحرج.

في هذه الرسالة تمت دراسة تأثير حجم المعوقات و الحرارة على كثافة التيار الحرج في مواد فائقة الموصلية ذوات درجة الحرارة الحرجة العالية و التي لها نظام دوري مربع من المعوقات. مع تغيير قوة المعوقات و حجم المعوقات و درجة الحرارة.

و أهم النتائج التي حصلنا عليها هي أن كثافة التيار الحرج في أي درجة حرارة تزداد مع زيادة حجم المعوقات. كما أنه في المعوقات ذات نصف القطر الصغير كثافة التيار الحرج تتناقص بسرعة مع زيادة درجة الحرارة، بينما في المعوقات ذات نصف القطر الكبير كثافة التيار الحرج تتناقص بعدل أبطأ. كما وجدنا أنه في درجات الحرارة المنخفضة هناك حد أعلى لتأثير حجم المعوقات في زيادة كثافة التيار الحرج. و قد كان هناك توافق بين النتائج التي حصلنا عليها النتائج العملية و النظرية.

جامعة الإمارات العربية المتحدة

عمادة الدراسات العليا

برنامج ماجستير علوم و هندسة المواد

أثر حجم المعوقات على كثافة التيار الحرج في المواد فائقة الموصلية ذوات درجة الحرارة الحرجة العالية

رسالة مقدمة من الطالبة:

سلامة بخيت سويدان النعيمي

إلى جامعة الإمارات العربية المتحدة

استكمالا لمتطلبات الحصول على درجة الماجستير في علوم و هندسة المواد

2006-2007